# Embryonic ablation of osteoblast *Smad4* interrupts matrix synthesis in response to canonical Wnt signaling and causes an osteogenesis-imperfecta-like phenotype

**Valerie S. Salazar[1,2], Nicholas Zarkadis[1], Lisa Huang[1], Jin Norris[1], Susan K. Grimston[1], Gabriel Mbalaviele[1] and Roberto Civitelli[1,*]**

[1]Washington University School of Medicine, Division of Bone and Mineral Disease, Departments of Internal Medicine and Cell Biology and Physiology, 660 South Euclid, Campus Box 8301, Saint Louis, MO 63110, USA
[2]Department of Developmental Biology at Harvard School of Dental Medicine, 188 Longwood Avenue, Boston, MA 02115, USA
*Author for correspondence (rcivitel@dom.wustl.edu)

*Accepted 7 August 2013*
*Journal of Cell Science 126, 4974–4984*

*doi: 10.1242/jcs.131953*

## Summary

To examine interactions between bone morphogenic protein (BMP) and canonical Wnt signaling during skeletal growth, we ablated *Smad4*, a key component of the TGF-β–BMP pathway, in *Osx1*$^{+}$ cells in mice. We show that loss of *Smad4* causes stunted growth, spontaneous fractures and a combination of features seen in osteogenesis imperfecta, cleidocranial dysplasia and Wnt-deficiency syndromes. Bones of *Smad4* mutant mice exhibited markers of fully differentiated osteoblasts but lacked multiple collagen-processing enzymes, including lysyl oxidase (*Lox*), a BMP2-responsive gene regulated by Smad4 and Runx2. Accordingly, the collagen matrix in *Smad4* mutants was disorganized, but also hypomineralized. Primary osteoblasts from these mutants did not mineralize *in vitro* in the presence of BMP2 or Wnt3a, and *Smad4* mutant mice failed to accrue new bone following systemic inhibition of the Dickkopf homolog Dkk1. Consistent with impaired biological responses to canonical Wnt, ablation of *Smad4* causes cleavage of β-catenin and depletion of the low density lipoprotein receptor Lrp5, subsequent to increased caspase-3 activity and apoptosis. In summary, *Smad4* regulates maturation of skeletal collagen and osteoblast survival, and is required for matrix-forming responses to both BMP2 and canonical Wnt.

**Key words:** Bone, Collagen, Osteoblast, Smad4, BMP, Wnt, β-catenin

## Introduction

Skeletal development and growth (bone modeling) depends upon the proliferation and differentiation of chondrocytes, the resorptive activity of osteoclasts, and the bone-forming function of osteoblasts. The coordinated actions of osteoblasts and osteoclasts further function to replace old bone in the mature skeleton (bone remodeling). Bone modeling and remodeling are controlled by molecular programs modulating proliferation, differentiation, function and survival of skeletal cells. Two key regulators of skeletal development and homeostasis are the bone morphogenic protein (BMP) and Wnt signaling systems. BMP2 and BMP4 are secreted ligands which are together necessary (Bandyopadhyay et al., 2006) and each sufficient (Kang et al., 2004; Wozney et al., 1988) to drive *de novo* bone formation by osteoblasts. Osteoblast-specific ablation of *Bmpr1a* or the downstream transcription factor *Smad4* decreases both bone formation and resorption (Kamiya et al., 2008a; Kamiya et al., 2008b; Mishina et al., 2004; Tan et al., 2007). Wnt ligands are secreted factors that signal through heteromeric receptor complexes comprising a Frizzled receptor and one of the low density lipoprotein receptors Lrp5 or Lrp6 (Nusse, 2005). Gain- or loss-of-function mutations of *LRP5* in humans result in high or low bone mass syndromes, respectively (Boyden et al., 2002; Gong et al., 2001; Little et al., 2002). In mice, the osteogenic effects of Lrp5 or Lrp6 activity derive largely, though not exclusively from β-catenin, which acts cell autonomously to specify osteoblast cell fate (Day et al., 2005; Hill et al., 2005; Ross et al., 2000), enhance osteoprogenitor proliferation (Rodda and McMahon, 2006), drive osteoblast differentiation and new bone formation (Hu et al., 2005; Rodda and McMahon, 2006), and regulate bone resorption through paracrine effects on osteoclasts (Glass et al., 2005).

Complex and sometimes contradictory interactions between BMP and Wnt/β-catenin signaling have been reported in the skeletal system. For example, BMPs can act upstream of canonical Wnt (Bain et al., 2003; Rawadi et al., 2003) in a manner that requires β-catenin (Chen et al., 2007; Hill et al., 2005). However, we and others have shown that osteogenic activity of β-catenin is suppressed by blocking BMP2 or BMP4, implying instead that BMPs act downstream of Wnt, or that the two pathways act cooperatively (Salazar et al., 2008; Winkler et al., 2005). Thus, simple epistatic models do not satisfactorily explain how BMP and Wnt/β-catenin signaling interact to drive osteogenesis. To further our understanding of the molecular mechanisms underlying BMP and Wnt/β-catenin interactions for skeletal growth and homeostasis, we generated mice with conditional ablation of *Smad4*, a key component of the greater TGF-β/BMP signaling system.

Using *Osx1-Cre* to drive *Smad4* ablation in differentiating osteoblasts we find, somewhat unexpectedly, far more severe skeletal abnormalities than previously reported with ablation restricted to mature osteoblasts (Tan et al., 2007). Loss of *Smad4* in $Osx1^{+}$ cells causes a pleiotropic phenotype consisting of a combination of features seen in Wnt-deficiency syndromes (Gong et al., 2001; Gong et al., 1996), cleidocranial dysplasia (Otto et al., 1997) and osteogenesis imperfecta (Forlino et al., 2011). This phenotype is caused by production of an abnormal collagen bone matrix and increased apoptosis in *Smad4*-deficient osteoblasts. We also find that *Smad4* deficiency renders bone cells resistant to matrix-mineralizing effects of the canonical Wnt pathway. Our study uncovers novel interactions between Smad4 with the Wnt/β-catenin system and Runx2, positioning Smad4 as a key modulator of multiple signaling pathways that control bone mass through the function of bone-forming cells.

## Results

### Severe growth retardation and spontaneous fracture in mice with deficiency of *Smad4* in $Osx1^{+}$ cells

Because pilot studies revealed that *Osx1*-driven *Smad4* ablation results in a far more severe phenotype than previously reported for a more restricted osteoblast *Smad4* deletion (Tan et al., 2007), an in-depth characterization of the skeletal phenotype was performed. At birth, $Smad4^{\Delta/\Delta}$ pups were slightly smaller than $Smad4^{F/F}$ (Fig. 1A), but were severely runted by postnatal day (P)28 (Fig. 1B). About 50% of $Smad4^{\Delta/\Delta}$ pups died by P14, and almost none survived to 8 weeks. Early lethality was not alleviated by access to paste-formula food or by keeping $Smad4^{\Delta/\Delta}$ pups with the mother. $Smad4^{+/\Delta}$ and $Smad4^{\Delta/\Delta}$ mice developed oral malocclusion (Fig. 1C,D), a trait observed in *Osx1-Cre* hemizygous mice (http://jaxmice.jax.org/strain/006361.html). However, dental abnormalities were far more severe in $Smad4^{\Delta/\Delta}$ mice, which exhibited yellow or even black dental discoloration typical of enamel hypoplasia (Fig. 1D). On whole-body 3D high-resolution microcomputed tomography (μCT) reconstructions at P28, $Smad4^{\Delta/\Delta}$ mice exhibited underdeveloped incisors (Fig. 1E, blue asterisk). And despite the presence of intact skeletal tissues observed during necropsy (Fig. 5D), μCT further revealed that the craniofacial and axial skeleton were severely under mineralized (Fig. 1E, red asterisks). Rib number was normal but the thoracic cavity was small. Multiple rib fractures, some with callus formation, were evident on plain radiographs at 8 weeks of age (Fig. 1F, red asterisks).

In the appendicular skeleton, $Smad4^{\Delta/\Delta}$ tibiae were small but morphologically normal (Fig. 2A,B). Trabecular bone, which is normally restricted to primary and secondary ossification centers, populated the entire diaphysis of $Smad4^{\Delta/\Delta}$ bones (Fig. 2B). In $Smad4^{\Delta/\Delta}$ mice at P28, tibias were 22.1±7.4% shorter (Fig. 2C), and bone mineral density (calculated as mineral content per unit volume of cortical bone) was reduced 20±3.8% relative to $Smad4^{F/F}$ mice (Fig. 2D). Trabecular bone volume as a function of trabecular tissue volume (BV/TV) in the metaphysis (first 30 slices below the growth plate) was not different between genotypes (Fig. 2E); but, when trabecular bone was instead quantified from the growth plate to the tibia-fibular junction, BV/TV was almost threefold higher in $Smad4^{\Delta/\Delta}$ than in $Smad4^{+/\Delta}$ or $Smad4^{F/F}$ mice (Fig. 2F). Thus, trabecular architecture at the metaphysis is appropriate for the smaller bone size of $Smad4^{\Delta/\Delta}$ mice, but their diaphyseal medullary space is inappropriately

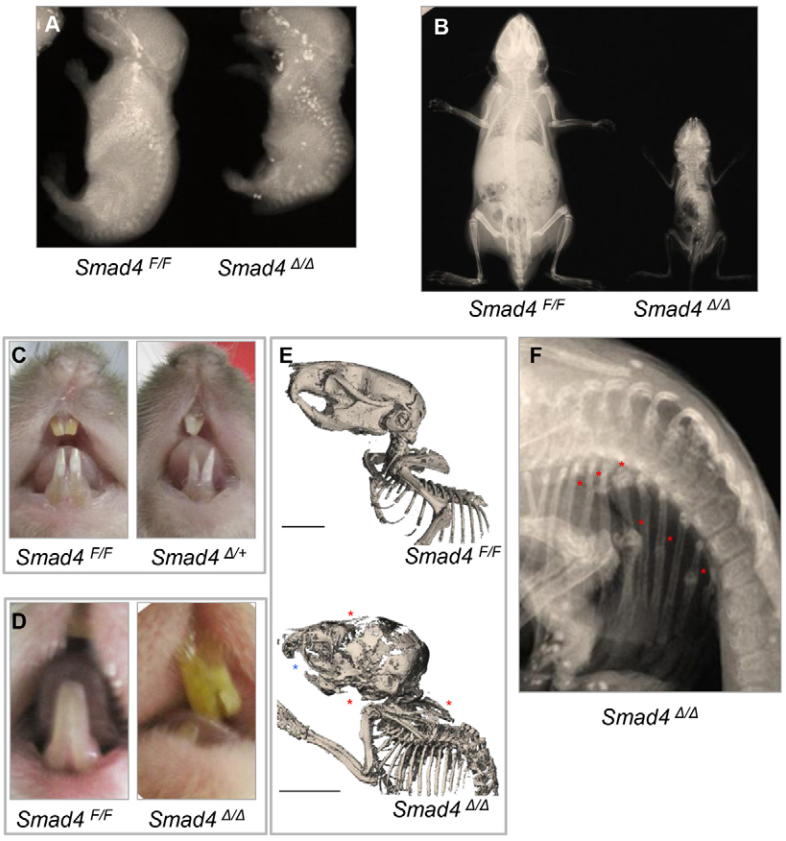


**Fig. 1. Skeletal phenotype of $Smad4^{F/F}$; *Osx1-Cre* Mice.** Contact radiographs of littermates at (A) P0 and (B) P28. (C,D) Malocclusion and enamel hypoplasia of the incisors. (E) 3D μCT reconstructions of skeletal structures in 4-week-old littermates. Scale bars: 5 mm. Blue asterisk indicates underdeveloped and hypomineralized incisors; red asterisks show severe hypomineralization of the craniofacial and axial skeleton. (F) Contact radiograph of an 8-week-old $Smad4^{\Delta/\Delta}$ mouse. Red asterisks indicate multiple rib fractures.

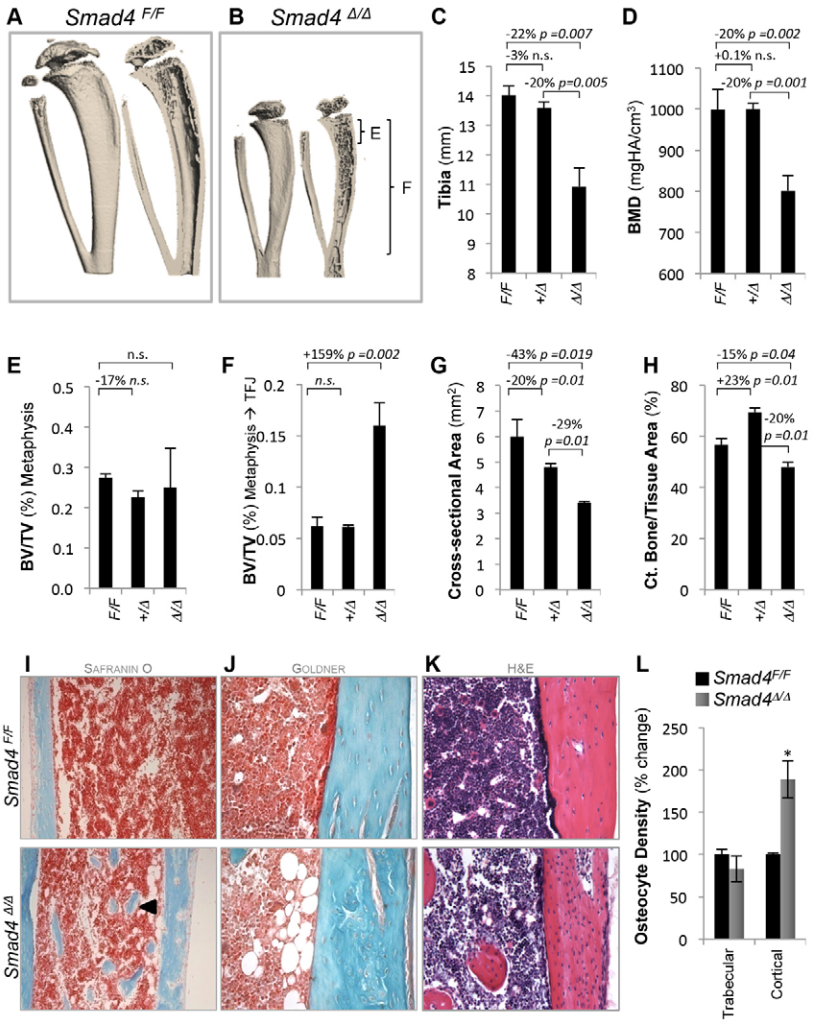


**Fig. 2. Bone structure of *Smad4*$^{F/F}$; *Osx1-Cre* Mice.** (A,B) 3D μCT reconstructions of tibiae of 4-week-old littermates, shown to scale. (C–H) Quantitative μCT analysis of the tibiae ($n \geq 4$ males/genotype). Data are means ± s.e.m., where *P* value is calculated versus *Smad4*$^{F/F}$ or *Smad4*$^{+/\Delta}$ and indicated by brackets. (C) Tibia length. (D) Mineral content per unit volume of cortical bone at the mid-diaphysis. (E,F) Volume of trabecular bone per volume of the trabecular compartment, calculated either in (E) the first 30 slices below the proximal growth plate or (F) from the proximal growth plate to the tibia/fibula junction. (G) Total peripheral cross-sectional area occupied by the diaphysis at mid-shaft. (H) Percentage of cross-sectional area occupied by cortical bone. (I) Safranin O staining of mid-sagittal sections of the tibia (10×). Black arrowhead shows diaphyseal trabeculae. (J) Goldner trichrome and (K) H&E staining on mid-sagittal sections of the tibia, mid-diaphysis (40×). (L) Osteocyte density was calculated per μm$^2$ of trabecular bone or cortical bone and was expressed as percentage change versus *Smad4*$^{F/F}$. Data are means ± s.e.m., where *$P<0.05$.

populated by an excessive amount of trabecular bone. Increased diaphyseal trabeculation was observed when deleting *Smad4* in *Bglap*$^{+}$ cells, and this was attributed to decreased osteoclastogenesis (Tan et al., 2007). Indeed, TRAP-positive osteoclasts were very sparse on the residual trabeculae, endocortical and periosteal surfaces of mutant *Smad4*$^{\Delta/\Delta}$ bones (supplementary material Fig. S3). *Smad4*$^{\Delta/\Delta}$ tibias were narrow at the mid-diaphysis with total cross-sectional tissue area reduced 43±1.3% relative to *Smad4*$^{F/F}$ and modestly reduced in *Smad4*$^{+/\Delta}$ mice (Fig. 2G). Relative to *Smad4*$^{F/F}$, cortical thickness (calculated as the percentage of total diaphyseal tissue area occupied by cortical bone) was also decreased in *Smad4*$^{\Delta/\Delta}$ tibias (15±1.5%, Fig. 2H). Cortical thickness was 23% higher in *Smad4*$^{+/\Delta}$, but this was the only abnormality evident in *Smad4*$^{+/\Delta}$ mice, and was the opposite of the defects observed in *Smad4*$^{\Delta/\Delta}$ mice. Notably, trabecular structures in the diaphysis of *Smad4*$^{\Delta/\Delta}$ tibiae were Safranin O negative and Fast Green positive (Fig. 2I), thus they are bone and not cartilage left behind during resorption of endochondral cartilage template. Goldner trichrome stain revealed that *Smad4*$^{\Delta/\Delta}$ cortical bone was primarily woven rather than lamellar (Fig. 2J). And, as evident from hemotoxylin and eosin staining (Fig. 2K), osteocyte density was significantly increased in the cortex of *Smad4*$^{\Delta/\Delta}$ relative to *Smad4*$^{F/F}$ bones, whereas no differences were seen in cancellous bone (Fig. 2L).

The *Osx1-Cre* transgene has been reported to cause skeletal abnormalities (Davey et al., 2012). At 4 weeks of age, *Osx1-Cre* tibiae were morphologically normal (supplementary material Fig. S2A,B) with a modest (~7%) decrease in length relative to wild-type littermates (supplementary material Fig. S2C). Bone mineral density measured by μCT was not altered (supplementary material Fig. S2D), and trabeculation was restricted to primary and secondary ossification centers as in wild-type mice (supplementary material Fig. S2B). Trabecular bone volume (BV/TV) in the metaphysis (first 30 slices below the growth plate) was reduced by ~36% in *Osx1-Cre* bones, although this did not reach statistical significance (supplementary material Fig. S2E). However, *Osx1-Cre* tibias were about 25% narrower at the mid-diaphysis relative to wild-type mice (supplementary material Fig. S2F) and cortical thickness was increased by about 14.5% (supplementary material Fig. S2G). These changes are inconsistent with the more severe phenotype evident in *Smad4*$^{\Delta/\Delta}$ mice.

### Smad4 modulates osteoblast responses to BMP and TGF-β

Loss of *Smad4* in *Osx1*$^{+}$ cells had no effect on the abundance of R-Smad mRNAs in marrow-free bone extracts (Fig. 3A); however, it sharply decreased the abundance of phosphorylated Smad1, Smad5 and Smad2 proteins (Fig. 3B). Smad3

phosphorylation was below detection in all genotypes (not shown). Total Smad1 and Smad2, but not Smad3 or Smad5 proteins, were sharply reduced in $Smad4^{\Delta/\Delta}$ bones (Fig. 3B) despite normal steady-state mRNA levels (Fig. 3A). Because both Smad1–Smad5 and Smad2–Smad3 signaling were affected by loss of *Smad4*, primary calvaria cells from neonatal mice were used to determine how *Smad4* regulates osteoblast differentiation, proliferation and survival in response to BMP2 or TGF-β. BMP2 increased BrdU incorporation by about 30%, and this effect was enhanced fourfold in the absence of *Smad4*, whereas TGF-β did not affect calvaria cell proliferation (Fig. 3C). Whereas basal levels of tissue non-specific alkaline phosphatase (ALP) activity were similar in $Smad4^{F/F}$ and $Smad4^{\Delta/\Delta}$ calvaria cells, the response to BMP2 stimulation of ALP activity was reduced about 50% in $Smad4^{\Delta/\Delta}$ cells. By contrast, ALP activity was inhibited about 70% by TGF-β in $Smad4^{F/F}$ cells and about 90% in $Smad4^{\Delta/\Delta}$ cells (Fig. 3D). In calvaria cells, TGF-β and BMP2 both reduced the number of $TUNEL^{+}$ and $DAPI^{+}$ nuclei (about 40 and 60%, respectively), which act as markers of apoptosis. Although loss of *Smad4* alone had no effect on *in vitro* apoptosis, it abolished the pro-survival effect of BMP2 and reduced that of TGF-β by ~50% (Fig. 3E).

### Abnormal collagen matrix and collagen-modifying enzymes in $Smad4^{\Delta/\Delta}$ bones

Growth retardation, hypomineralization of bone and teeth, propensity to fracture and increased osteocyte density are hallmarks of osteogenesis imperfecta (Forlino et al., 2011), raising the possibility that $Smad4^{\Delta/\Delta}$ osteoblasts either do not differentiate or that they do mature but are unable to secrete a normal bone matrix. Despite the report of an osteoblast differentiation defect upon *Bglap*-driven ablation of *Smad4* (Tan et al., 2007), we found that mRNA levels of early osteoblast genes, *Runx2* and *Osx1*, as well as genes prevalently expressed in osteocytes, *Dmp1* and *Phex* were unaltered in $Smad4^{\Delta/\Delta}$ bones (Fig. 4A). Likewise, genes involved in osteoblast maturation and bone matrix production, such as *Alp1* (tissue non-specific alkaline phosphatase), *Spp1* (osteopontin) and *Ibsp* (bone sialoprotein) were also unaffected *in vivo* by *Smad4* deletion. Expression of both *Col1A1* and *Bglap* (osteocalcin) was 32% lower in $Smad4^{\Delta/\Delta}$ relative to $Smad4^{F/F}$, although the difference did not reach statistical significance (Fig. 4B). Nonetheless, histologic sections of $Smad4^{\Delta/\Delta}$ tibiae from 6-week-old littermate mice stained with Picrosirius Red and examined under polarized light emitted a red/yellow light (Fig. 4Ciii,iv) compared with the prevalently green color emitted by trabecular and cortical bone of $Smad4^{F/F}$ (Fig. 4Ci,ii), indicating that thickness or packing density of collagen fibers is abnormal (Dayan et al., 1989). Together, these data indicate that differentiation of *Smad4*-deficient osteoblasts was delayed (Fig. 3D), but not blocked (Fig. 4A,B), and furthermore, that *Smad4*-deficient osteoblasts did not function properly, depositing abnormal collagen into the skeletal extracellular matrix. Accordingly, three collagen-processing enzymes, prolyl 4-hydroxylase, alpha subunit III (*P4Ha3*), procollagen-lysine, 2-oxoglutarate 5-dioxygenase 3 (*Plod3*) and lysyl oxidase (*Lox*) were sharply downregulated in $Smad4^{\Delta/\Delta}$ mice (Fig. 4D). Plod3 and P4Ha3 are required for collagen triple helix formation, and Lox mediates covalent crosslinking between collagen fibrils, a crucial step required for the structural integrity of a collagen matrix (Trackman, 2005).

### Smad4 and Runx2 regulate *Lox* transcription

Among the three collagen-processing enzymes noted above, only *Lox* mRNA was acutely upregulated in MC3T3s by overnight stimulation with BMP2; both *Plod3* and *Lox* were significantly upregulated by TGF-β, although the induction was modest (supplementary material Figs S4A–C). Thus, we narrowed our focus to *Lox*. *In vivo*, Lox protein was significantly diminished in conditional heterozygous $Smad4^{+/\Delta}$ bones, and it was almost undetectable in $Smad4^{\Delta/\Delta}$ bones. Osterix and β-actin were unchanged across genotypes (Fig. 5A). To determine whether

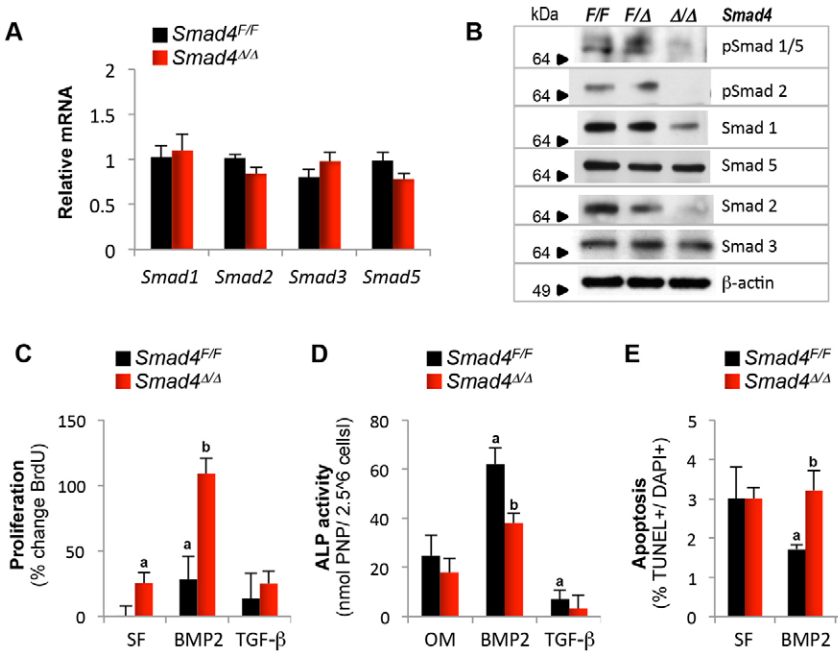


**Fig. 3. *Smad4* regulates how osteoblasts respond to BMP2 and TGF-β.** (A) qPCR on marrow-free bone. $n=7$ for $Smad4^{F/F}$ and $n=4$ for $Smad4^{\Delta/\Delta}$. (B) Immunoblot on marrow-free bone. (C–E) Cell-based assays using primary calvaria cells from neonatal mice. (C) Primary calvaria cells were seeded to 70% confluence, serum-deprived overnight, and then mitotic cells were labeled for 2 hours with BrdU in serum-free medium (SF) ± BMP2 (200 ng/ml) or TGF-β (10 ng/ml). (D) Primary calvaria cells were seeded to peak confluence and cultured in osteogenic medium (OM) ± BMP2 (200 ng/ml) or TGF-β (10 ng/ml). ALP activity was measured on day 7. (E) Primary calvaria cells were cultured overnight in serum-free medium (SF) ± BMP2 (200 ng/ml) or TGF-β (10 ng/ml). Apoptosis was quantified by calculating the percentage of $TUNEL^{+}$ and $DAPI^{+}$ cells. $n\geq500$ cells per measurement with three replicates. All numerical data are expressed as means ± s.e.m., where $^{a}P<0.05$ versus $Smad4^{F/F}$ cells in control medium (serum-free or osteogenic); $^{b}P<0.05$ versus $Smad4^{F/F}$ cells in BMP2; $^{c}P<0.05$ versus $Smad4^{F/F}$ cells in TGF-β.

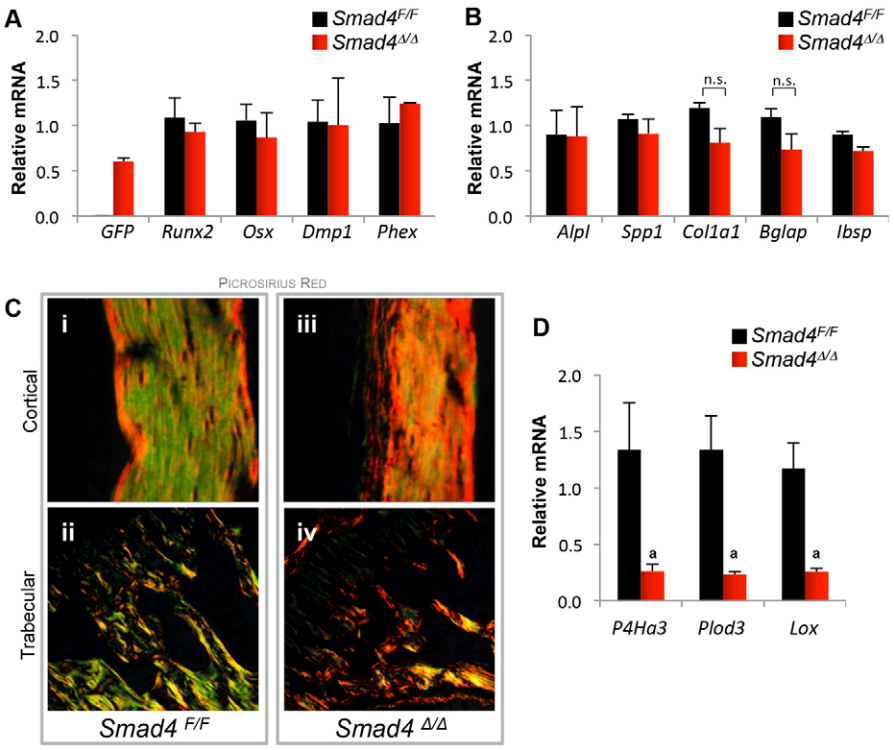


**Fig. 4. *Smad4* regulates the collagen biosynthetic pathway in bone.** (A,B,D) qPCR on marrow-free bone. (A) Osteoblast differentiation markers. (B) Extracellular matrix components. (D) Collagen-modifying enzymes. Data are expressed as means ± s.e.m., where $^{a}P<0.05$ versus $Smad4^{F/F}$. $n=7$ for $Smad4^{F/F}$ and $n=4$ for $Smad4^{\Delta/\Delta}$. (C) Picrosirius Red stain and polarized light microscopy on mid-sagittal sections of the tibia from 6-week-old littermates. (i) and (iii) are 40× magnifications of cortical bone. (ii) and (iv) are 10× magnifications of trabecular bone at the proximal tibial metaphysis.

induction of *Lox* by BMP2 is dependent on *Smad4*, we transfected MC3T3 calvaria cells with *Smad4* siRNA, which reduced *Smad4* expression ~70% (Fig. 5B) and inhibited BMP2 responsiveness of a luciferase reporter containing 12 tandem Smad-binding elements (Smad-luciferase; supplementary material Fig. S4D). Both basal and BMP2-stimulated (~5.5-fold) *Lox* mRNA expression was significantly inhibited (about 50% and 80%, respectively) by *Smad4* siRNA (Fig. 5B). Because the murine *Lox* promoter contains ≥9 putative Smad-binding elements (supplementary material Fig. S5), we determined whether Smad4 binds to the *Lox* promoter by performing chromatin immunoprecipitation (ChIP) on MC3T3 nuclear extracts. Using qPCR primers targeted to the −252 bp 5′ region of the *Lox* promoter, we found that Smad4 antibody

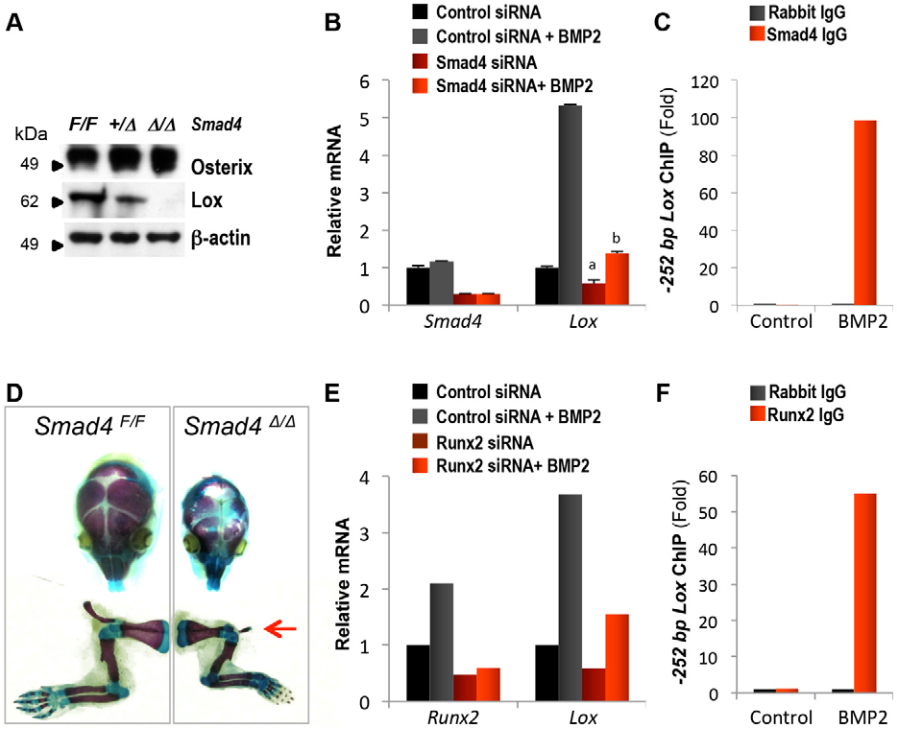


**Fig. 5. *Lox* is a BMP2-responsive gene regulated by Smad4 and Runx2.** (A) Immunoblot on marrow-free bone. (B) qPCR on MC3T3s transfected with non-targeted or *Smad4* siRNA and treated for 72 hours ± BMP2 (200 ng/ml). Data are means ± s.e.m., where $^{a}P<0.05$ versus control siRNA and $^{b}P<0.05$ versus control siRNA + BMP2. Experiments were performed three times with three replicates. (C) Smad4 or Rabbit IgG was used to perform chromatin immunoprecipitation from MC3T3 cells treated for 72 hours ± BMP2 (200 ng/ml). *Lox* promoter fragments were quantified by qPCR. (D) Alizarin Red and Alcian Blue whole-mount stains on neonates, shown to scale. (E) qPCR on MC3T3s transfected with non-targeted or *Runx2* siRNA and treated for 72 hours ± BMP2 (200 ng/ml). (F) Runx2 or Rabbit IgG was used to perform chromatin immunoprecipitation on MC3T3 cells treated for 72 hours ± BMP2 (200 ng/ml). *Lox* promoter fragments were quantified by qPCR.

precipitated 99-times more *Lox* promoter fragments from the chromatin of BMP2-treated cells relative to untreated cells (Fig. 5C), demonstrating that Smad4 is recruited to the *Lox* promoter in response to BMP2.

Intriguingly, *Smad4*$^{\Delta/\Delta}$ mice exhibited hypomineralized interparietal bones and clavicle hypoplasia, features evident at birth by whole-mount skeletal preparations (Fig. 5D) and by μCT of 4-week-old littermates (supplementary material Fig. S4E). This combination of features is a hallmark of cleidocranial dysplasia, a condition linked to *Runx2* haploinsufficiency (Mundlos et al., 1997; Otto et al., 1997). Because *Runx2* mRNA was expressed at normal levels in *Smad4*$^{\Delta/\Delta}$ bones (Fig. 4A), we considered the possibility that at least part of the phenotype of *Smad4*$^{\Delta/\Delta}$ mice arises from disruption of Runx2 transcriptional activity. In fact, the Lox promoter contains ≥8 putative Runx2-binding elements interspersed with Smad4 binding elements (supplementary material Fig. S5); thus, we tested whether BMP2 acts through both Smad4 and Runx2 to regulate expression of *Lox* in osteoblasts. We first used the OSE2-Luc reporter, which contains six Runx2 responsive elements (Ducy and Karsenty, 1995) to demonstrate that Runx2 transcriptional activity in MC3T3s is sensitive to BMP2 (supplementary material Fig. S4F). qPCR showed that *Runx2* mRNA is upregulated ~twofold in MC3T3s by BMP2. We decreased *Runx2* mRNA ~53% in control cells and ~71% in BMP2-treated cells by treating cells with *Runx2* siRNA. *Runx2* siRNA diminished steady-state levels of *Lox* mRNA by ~42%, and attenuated BMP2 stimulation of *Lox* expression by ~80% (Fig. 5E). In ChIP assays, Runx2 antibody precipitated ~55-times more *Lox* promoter fragments from nuclear extracts of BMP2-treated cells than from untreated cells (Fig. 5F). Neither Smad4 nor Runx2 antibodies immunoprecipitated promoter fragments of *Rpl30*, a control gene promoter (supplementary material Fig. S4G). Therefore, both Smad4 and Runx2 are recruited to the *Lox* promoter in response to BMP2. Loss of either Smad4 or Runx2 is sufficient to impair *Lox* expression upon BMP2 stimulation.

## Smad4 maintains the mineralizing response to canonical Wnt signaling

Although defective collagen processing can explain some of the osteogenesis-imperfecta-like features, it is probably not the only cause of the severe skeletal growth and delayed ossification defects present in *Smad4*$^{\Delta/\Delta}$ mice. As noted, the BMP and Wnt/β-catenin pathways intersect at different levels in bone cells (Chen et al., 2007; Rawadi et al., 2003), and we and others find that BMP2 and BMP4 signaling is permissive for the osteogenic effect of β-catenin (Salazar et al., 2008; Winkler et al., 2005). Hence, we tested whether loss of *Smad4* affects how osteoblasts respond to Wnt/β-catenin signaling. Consistent with normal expression of *Alp1* in bones from 4-week-old *Smad4*$^{\Delta/\Delta}$ mice (Fig. 4B), bone marrow stromal cells (BMSCs) from *Smad4*$^{\Delta/\Delta}$ mice developed normal levels of alkaline phosphatase activity when grown for 28 days in osteogenic medium; but, in contrast to *Smad4*$^{F/F}$ cells, no further increase was observed after exposure to Wnt3a in the mutant cells (Fig. 6A). More to the point, whereas BMP2 and Wnt3a potently stimulated deposition of mineralized matrix in control BMSCs, no such response was observed in *Smad4*$^{\Delta/\Delta}$ cells in the presence of either factor (Fig. 6B). To determine whether insensitivity of *Smad4*$^{\Delta/\Delta}$ cells to Wnt3a reflects *in vivo* resistance to Wnt signaling, we used a

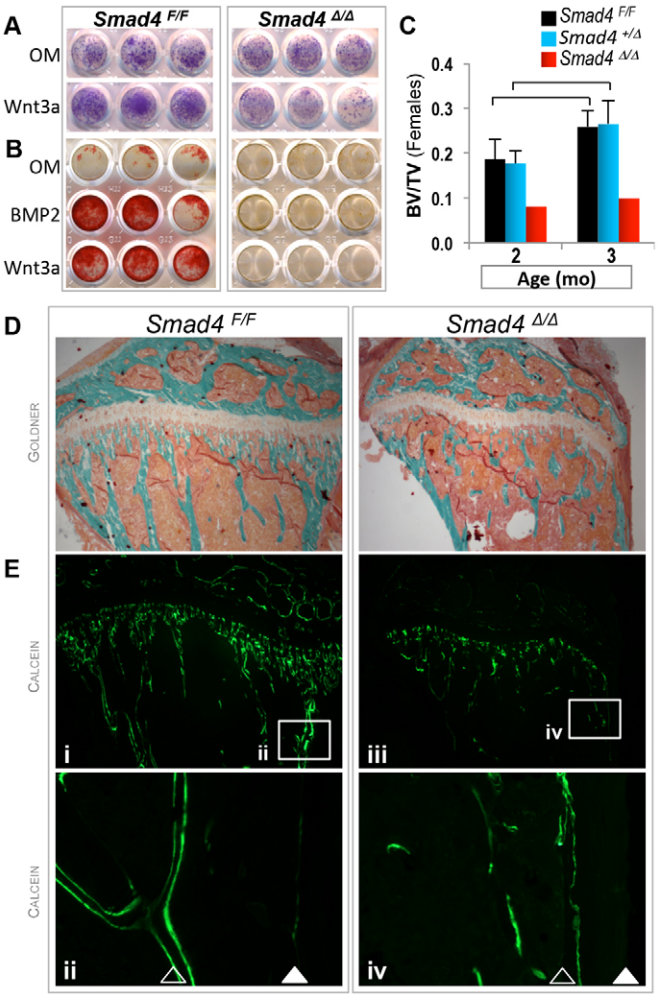


**Fig. 6. *Smad4* is required for mineralizing responses to BMP2 and Wnt3a.** (A) Alkaline phosphatase activity and (B) Alizarin-Red-positive nodules in bone marrow stromal cells cultured for (A) 28 days or (B) 10 days in osteogenic medium (OM) ± BMP2 (200 ng/ml) or Wnt3a (25 ng/ml). (C) Effect of anti-Dkk1 (20 mg/kg/day, i.p. three times/week, 4 weeks) on trabecular bone mass at the proximal tibia of female mice, assessed before and after treatment by *in vivo* μCT. $n=7$ for *Smad4*$^{F/F}$, $n=6$ for *Smad4*$^{+/\Delta}$ and $n=1$ for *Smad4*$^{\Delta/\Delta}$. Data are means ± s.e.m., where brackets indicate $P<0.05$. (D) Goldner trichrome stain and (E) calcein labeling on serial sections of the tibia from Smad4$^{F/F}$ (left) or *Smad4*$^{\Delta/\Delta}$ (right) mice after 4 weeks of anti-Dkk1 treatment. (i) and (iii) are 4× magnification; (ii) and (iv) are 40× magnification, representing boxed areas in (i) and (iii). Open arrowheads indicate endosteal surface, closed arrowheads show periosteal surface. Note lack of second calcein label on endosteal surface of *Smad4*$^{\Delta/\Delta}$ [open arrowhead in (iv)].

Dkk1 neutralizing antibody (αDkk1) that has been shown to induce bone formation when given systemically to mice with rheumatoid arthritis (Diarra et al., 2007). Treatment with αDkk1 (20 mg/kg/day, i.p. three times/week, 4 weeks) produced about 40% and 50% increments of trabecular bone mass in female *Smad4*$^{F/F}$ and *Smad4*$^{+/\Delta}$ mice, respectively, whereas no accrual of bone mass occurred in one *Smad4*$^{\Delta/\Delta}$ female that survived the 4 week treatment to 3 months of age (Fig. 6C). Abundant double calcein labels were present in *Smad4*$^{F/F}$ tibiae after αDkk1 treatment (Fig. 6Ei,ii), whereas only a few labeled surfaces with

no double labels were observed in the *Smad4*$^{\Delta/\Delta}$ tibia (Fig. 6Eiii,iv). Goldner trichrome stain was used for orientation on serial sections (Fig. 6D). This was recapitulated in a pair of male *Smad4*$^{\Delta/\Delta}$ and *Smad4*$^{F/F}$ littermate mice (supplementary material Fig. S6).

To understand the molecular mechanisms of Wnt resistance in *Smad4*$^{\Delta/\Delta}$ mice and cells, components of the Wnt pathway were analyzed by immunoblot on marrow-free bone extracts (Fig. 7A). Lrp5 was barely detectable in *Smad4*$^{\Delta/\Delta}$ relative to *Smad4*$^{F/F}$ and *Smad4*$^{+/\Delta}$ bones, whereas Lrp6 abundance was normal. Total and phospho-GSK3β were unaffected by loss of *Smad4*, as was phosphorylation of GSK3β-target residues on β-catenin. However, an antibody against the β-catenin N-terminus revealed fainter immunoreactive bands (82–115 kDa) in *Smad4*$^{\Delta/\Delta}$ relative to *Smad4*$^{F/F}$ and *Smad4*$^{+/\Delta}$ bone extracts. Likewise, multiple bands were also revealed in *Smad4*$^{F/F}$ and *Smad4*$^{+/\Delta}$ bone using an antibody recognizing the C-terminus of β-catenin; however, these bands were barely detectable in the *Smad4*$^{\Delta/\Delta}$ lane, where a faster migrating band became far stronger (Fig. 7A). Truncation of β-catenin C-terminus deactivates its transcriptional activity (Cong et al., 2003); indeed, mRNAs of the β-catenin target genes *EphB4* (Batlle et al., 2002) and *Ccnd1* (Tetsu and McCormick, 1999) were downregulated ~70% and ~50%, respectively in *Smad4*$^{\Delta/\Delta}$ bone. However, the abundance of mRNAs for *Lrp5*, *Lrp6* and *Catnnb* were unaffected by *Smad4* genotype (Fig. 7B). The discrepancy between mRNA and protein data suggests that embryonic ablation of *Smad4* triggers a GSK3β-independent mechanism of β-catenin degradation. As shown in Fig. 7C, two Caspase-3 cleavage sites reside within the C-terminal transactivation domain of β-catenin; three sites are in the N-terminal regulatory domain (Hunter et al., 2001). Indeed, *Smad4*$^{\Delta/\Delta}$ bones contain high levels of activated (cleaved) Caspase-9 and Caspase-3, relative to *Smad4*$^{F/F}$ and *Smad4*$^{+/\Delta}$ bone. Substantiating increased caspase activity, cleaved PARP, a known substrate of Caspase-3, was far more abundant *Smad4*$^{\Delta/\Delta}$ bones relative to controls (Fig. 7D). Consistent with the earlier observation (Fig. 7A), when intact femurs from 4-week-old *Smad4*$^{\Delta/\Delta}$ male mice are cultured *ex vivo* in osteogenic medium, the abundance of full-length β-catenin was decreased relative to *Smad4*$^{F/F}$ bones, whereas the abundance of faster-migrating bands increased. Importantly, the intensity of these slower-migrating bands reactive to the C-terminus β-catenin antibody was significantly reduced in the presence of the caspase-3 inhibitor, Z-DEVD-fmk (Fig. 7E, red arrowhead), suggesting these are in fact cleavage products of activated Caspase-3. *In vivo*, there were abundant TUNEL$^{+}$ osteoblasts and osteocytes in focal aggregates on the diaphysis of *Smad4*$^{\Delta/\Delta}$ bones (Fig. 7F). *In*

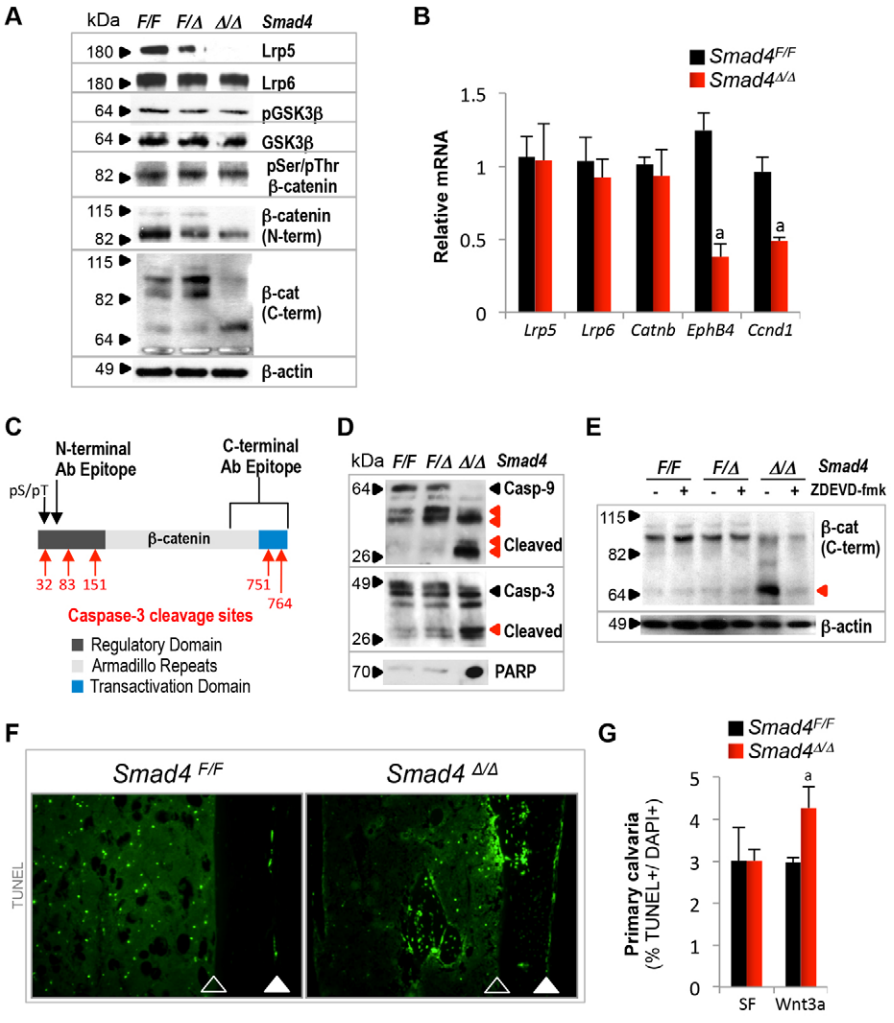


**Fig. 7. Diminished osteoblast survival and Caspase-3-associated cleavage of β-catenin.** (A) Immunoblot or (B) qPCR analysis of Wnt pathway in marrow-free bone. Data are means ± s.e.m., where $^{a}P<0.05$ versus *Smad4*$^{F/F}$. $n=7$ for *Smad4*$^{F/F}$ and $n=4$ for *Smad4*$^{\Delta/\Delta}$. (C) Schematic of β-catenin showing relative positions of antibody epitopes recognized in A and Caspase-3 cleavage sites. (D) Immunoblot on marrow-free bone. (E) Intact femurs from 4-week-old littermates were cultured *ex vivo* for 12 hours in osteogenic media + DMSO or Z-DEVD-fmk (100 μM). Immunoblot was performed on marrow-free bone. (F) Immunofluorescence for TUNEL$^{+}$ cells in the tibiae in 4-week-old littermates (10×). Open arrows indicate endosteum and closed arrows show periosteum. (G) Primary calvaria cells were cultured overnight in serum-free medium (SF) ± Wnt3a (25 ng/ml). Apoptosis was quantified by calculating the percentage of TUNEL$^{+}$ and DAPI$^{+}$ cells. Means ± s.e.m., $n\geq500$ cells per measurement with three replicates. $^{a}P<0.05$ versus *Smad4*$^{F/F}$ in Wnt3a.

*vitro*, exposure to Wnt3a had no effect on the percentage of $Smad4^{F/F}$ BMSC that underwent apoptosis after serum deprivation. However, Wnt3a increased the percentage of TUNEL$^{+}$ $Smad4^{\Delta/\Delta}$ BMSC by almost 50% (Fig. 7G), providing a likely explanation as to why $Smad4^{\Delta/\Delta}$ BMSCs differentiated for 2–4 weeks in the presence of Wnt3a appeared less dense, despite being initially seeded at peak confluence and in equal number to $Smad4^{F/F}$ cells (Fig. 6A).

## Discussion

This work reveals novel and unexpected functions of *Smad4* in bone. We show that *Smad4* is necessary in $Osx1^{+}$ cells for skeletal development, longitudinal bone growth and production of normal bone matrix. These diverse functions of *Smad4* are linked to its ability to interface with Runx2 and to regulate canonical Wnt signaling. Specifically, loss of *Smad4* in $Osx1^{+}$ bone cells disrupts expression of an essential Runx2 gene target and causes β-catenin cleavage associated with caspase-3 activation.

The phenotype resulting from *Smad4* ablation in $Osx1^{+}$ cells represents a combination of features present in different genetic disorders. Severe growth defects, propensity to fracture, dental enamel defects, fibrillar collagen abnormalities and increased osteocyte density are features of osteogenesis imperfecta (Forlino et al., 2011). Although *Col1A1* mutations are responsible for most cases of the disease, absence of collagen-processing enzymes has been linked to recessive forms (Forlino et al., 2011). *P4Ha3*, *Plod3* and *Lox* are all severely deficient in $Smad4^{\Delta/\Delta}$ mice. Although none of these genes has been linked to osteogenesis imperfecta, *Plod3* mutations have been found in subjects with low bone mass and features of Ehlers-Danlos syndrome, a condition also characterized by connective tissue matrix defects (Salo et al., 2008). Furthermore, Ehlers-Danlos type VI, with kyphoscolisis and tissue fragility, is caused by loss-of-function mutations of *Plod1* (Beighton et al., 1998). Hence, it is conceivable that the compound deficiency of multiple collagen-processing enzymes accounts for the osteogenesis-imperfecta- and Ehlers-Danlos-like features of $Smad4^{\Delta/\Delta}$ mice. Notably, *Lox*-null mice exhibit normal skeletal patterning at birth; however, the skeleton is extremely fragile, collagen fiber size is altered, and *Lox*-null osteoblasts do not mineralize well (Pischon et al., 2009), conditions also present in $Smad4^{\Delta/\Delta}$ mice. Because *Lox*-null mice die perinatally, it is not yet clear whether other lysyl-oxidase-like enzymes can compensate for Lox, or whether *Lox* deficiency alone can retard growth (Nishioka et al., 2012). Interestingly, the growth defect in $Smad4^{Osx1\Delta/\Delta}$ mice is far more severe than reported in $Smad4^{Ocn\Delta/\Delta}$ mice (Tan et al., 2007). Since *Osx1-Cre* has been shown to recombine in pre-hypertrophic chondrocytes of the growth plate (Maes et al., 2010), the longitudinal growth defect in $Smad4^{Osx1\Delta/\Delta}$ mice is likely to be the result of *Smad4* ablation in the growth plate (Retting et al., 2009; Zhang et al., 2005). Indeed, BrdU histology reveals a more than 90% decrease in proliferation of growth plate chondrocytes of 4-week-old $Smad4^{\Delta/\Delta}$ mice relative to $Smad4^{F/F}$ littermates (data not shown).

We focused on *Lox* to study the molecular action of Smad4 in osteoblasts because *Lox* is acutely regulated by BMP2, is a key enzyme of the collagen biosynthetic pathway and collagen abnormalities represent a novel feature of *Smad4* deficiency. We found that *Lox* is regulated directly by Smad4 and Runx2, and that each transcription factor is required but not sufficient in the absence of the other for induction of *Lox* in osteoblasts by BMP2. Thus, Smad4 and Runx2 act cooperatively to regulate *Lox* transcription. Consistent with the contribution of Runx2 to Smad4 activity, $Smad4^{\Delta/\Delta}$ mice also exhibit skeletal features reminiscent of cleidocranial dysplasia (skull hypomineralization, clavicle hypoplasia), a condition caused by *Runx2* haploinsufficiency (Otto et al., 1997). Such features are not present in TGF-β mutant mice, but are reported in mice with osteoblast-specific ablation of BMP2 and BMP4 (Bandyopadhyay et al., 2006) or TAK1 and p38 (Greenblatt et al., 2010), a pathway used by BMPs to activate Runx2 transcriptional activity. Altogether, these data support the notion that BMP2 and BMP4 act through Smad4 and Runx2 to regulate collagen crosslinking during skeletal development.

We also made the novel observation that *Smad4* is required for the mineralizing stimulus of canonical Wnt signaling. Interactions between BMP and Wnt/β-catenin pathways have been reported, sometimes with divergent findings (Bain et al., 2003; Rawadi et al., 2003; Salazar et al., 2008; Winkler et al., 2005). Our earlier data show that BMP signaling is required for induction of osteoblast differentiation and mineralization by β-catenin (Salazar et al., 2008). Here, $Smad4^{\Delta/\Delta}$ osteoblasts failed to mineralize in response to not only BMP2, but also Wnt3a; and $Smad4^{\Delta/\Delta}$ mice failed to activate bone formation in response to systemic Wnt activation by Dkk1 antibody. The mechanisms for such insensitivity of *Smad4*-deficient cells and animals to Wnt are complex, but the major abnormalities are downregulation of Lrp5, and β-catenin cleavage by activated caspase-3. Interruption of canonical Wnt signaling probably contributes to the very low bone mineral content of $Smad4^{\Delta/\Delta}$ mice, compounding Smad4- and Runx2-dependent defects in collagen processing. Importantly, analysis of $Smad4^{\Delta/\Delta}$ bones shows that although osteoblast survival and collagen processing are defective, bone-forming cells retain their ability to undergo full differentiation. Thus, whereas *Smad4* is dispensable in $Osx1^{+}$ osteoblasts for further progression along their lineage, osteoblasts in $Smad4^{\Delta/\Delta}$ bones do not properly use Runx2 signaling to drive collagen matrix maturation, undergo caspase-3 mediated cleavage of β-catenin and are susceptible to apoptosis. Consequently, by 4 weeks of age, canonical Wnt signals are dampened following embryonic ablation of *Smad4*, leaving $Smad4^{\Delta/\Delta}$ osteoblasts resistant to the osteogenic stimulus of both BMP2 and Wnt proteins (Fig. 8). Because *Smad4* is deleted in $Osx1^{+}$ cells, loss of β-catenin occurs after the crucial Runx2–Osx1 transition point for which β-catenin is absolutely required (Rodda and McMahon, 2006), explaining why osteoblasts differentiate in these $Smad4^{\Delta/\Delta}$ mice despite β-catenin cleavage.

In the absence of tetracycline repression, the primary recombination event in *Osx1-Cre* models occurs between embryonic day (E)14.5 and birth (Rodda and McMahon, 2006). Since we did not delay recombination with tetracycline, the bone extracts we analyzed from 4- to 6-week-old mice are expected to be composed largely of mature osteoblasts and osteocytes derived from progenitors that lost *Smad4* during embryonic skeletogenesis. Thus, our western blot and qPCR data reflect a homeostatic state achieved several weeks after the loss of *Smad4*, and might be distinct from the effects of acute or postnatal recombination of Smad4. Indeed, time-course cultures of osteoblasts made from calvaria of newborn mice indicate that some molecular events such as depletion of β-catenin commence over time, not immediately (data not shown).

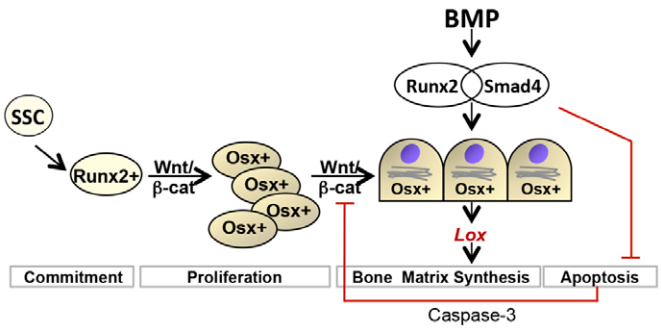


**Fig. 8. *Smad4* is dispensable in *Osx1*$^{+}$ cells for the formation of fully differentiated *Dmp1/Phex*$^{+}$ osteoblasts in bone.** However, *Smad4*-deficient osteoblasts do not properly drive collagen matrix maturation, exhibit reduced mineralizing activity, and are more susceptible to cell death. By 4 weeks of age, *Smad4*$^{\Delta/\Delta}$ mice exhibit extensive apoptosis of osteoblasts in bone, with evidence of Caspase-3-associated cleavage of β-catenin. Protein levels of the Wnt receptor Lrp5 are also critically low in *Smad4*$^{\Delta/\Delta}$ bones. Consequently, anabolic responses to canonical Wnt signaling are dampened following constitutive embryonic ablation of *Smad4*, leaving *Smad4*$^{\Delta/\Delta}$ osteoblasts resistant to the osteogenic stimulus of both BMP2 and Wnt proteins.

A potential limitation of our study is that the *Osx1-Cre* transgene affects cortical structure by itself, and could account for the modest decrease in tibia length and mild cortical abnormalities observed in conditional heterozygous *Smad4*$^{+/\Delta}$ mice, which also carry the *Osx1-Cre* transgene. However, the changes observed in *Smad4*$^{\Delta/\Delta}$ mice are different, far more severe than in *Smad4*$^{+/\Delta}$ mice, and also affect cancellous bone; thus, they probably represent a true effect of *Smad4* ablation. Skeletal abnormalities are not reported in *Smad4*$^{F/F}$ mice in the absence of a *Cre* allele (Tan et al., 2007; Zhang et al., 2005) and structural μCT parameters of *Smad4*$^{F/F}$ bones fall within expected values for wild-type mice on a mixed strain background (Di Benedetto et al., 2010).

In summary, *Smad4* is a key regulator of skeletal development and homeostasis, affecting the function and survival of bone-forming cells. Genetic ablation of *Smad4* in *Osx1*$^{+}$ cells results in a complex and severe phenotype characterized by growth retardation, dental enamel hypoplasia, skeletal hypomineralization, abnormalities of collagen matrix and spontaneous fractures. Our findings suggest that dysfunction of BMP signaling through Smad4 might be involved in the pathogenesis of some forms of osteogenesis imperfecta or Ehlers–Danlos syndromes. We also uncover novel interactions between *Smad4* and crucial osteoblast signaling systems, specifically Runx2 and Wnt/β-catenin, demonstrating that *Smad4* in osteoblasts is necessary for the osteogenic actions of both BMP2 and canonical Wnt proteins.

## Materials and Methods

### Materials

Rat monoclonal anti-mouse Dkk1 (clone 11H10, Lot 14073109), a gift from Dr William Richards, Amgen (Thousand Oaks, CA), was prepared in sterile saline and administered at 20 mg/kg/day by intra-peritoneal injections, three times a week for 4 weeks. All chemicals and reagents, unless specified otherwise, were obtained from Sigma Aldrich. Antibodies are listed in supplementary material Table S1.

### Mice

*Osx1-GFP::Cre (Osx1-Cre)* transgenic mice express GFP::Cre in *Osx1*$^{+}$ cells (Rodda and McMahon, 2006). *Rosa26R*$^{flox(lacZ)}$ reporter alleles *(R26R*$^{F}$*)* express β-galactosidase in Cre$^{+}$ cells (Soriano, 1999). Conditional *Smad4* alleles *(Smad4*$^{F}$*)* undergo Cre-mediated excision of a floxed exon 8. *Osx1-Cre* hemizygous mice (*Osx1-Cre*$^{Tg/0}$) were mated with *Rosa26R*$^{flox(lacZ)}$ homozygous mice to verify by *lacZ* staining that the *Osx1-Cre* transgene targets cortical and trabecular osteoblasts and osteocytes, but not bone marrow cells (supplementary material Fig. S1A). To conditionally ablate *Smad4*, *Osx1-Cre*$^{Tg/0}$ mice were crossed to *Smad4*$^{F/F}$ mice. *Osx1-Cre*$^{Tg/0}$*; Smad4*$^{+/F}$ (*Smad4*$^{+/\Delta}$) males were crossed to *Smad4*$^{F/F}$ females to generate *Osx1-Cre*$^{Tg/0}$*; Smad4*$^{F/F}$ (*Smad4*$^{\Delta/\Delta}$ or cKO) and *Smad4*$^{F/F}$ (wild-type control). The *Osx1-Cre* mouse model incorporates a Tet-OFF regulatory mechanism. However, tetracycline-mediated repression was not used in these studies. Demonstrating efficient gene recombination, *Smad4*$^{F/F}$ mice show Smad4 immunohistochemical staining in cells adherent to trabecular structures in the primary spongiosa, whereas there is no detectable Smad4 staining around the trabecular structures in *Smad4*$^{\Delta/\Delta}$ (supplementary material Fig. S1B). Some visible signal appears immediately below the growth plate, and might represent Smad4 in osteoclasts, which are abundant in subchondral bone and are not targeted by *Osx1-Cre*. Smad4 protein is nearly undetectable in marrow-free bone extracts of *Smad4*$^{\Delta/\Delta}$ versus *Smad4*$^{F/F}$ (supplementary material Fig. S1C). Mice were in a mixed C57BL/6-C129/J background, fed regular chow *ad libitum*, and housed at 25°C with 12 hour light/dark cycles. All studies were approved by the Animal Studies Committee of Washington University in St Louis.

### Histology

#### *lacZ*

Whole bones were fixed for 1 hour in 54 μl of 10% NBF and 0.8 μl of 25% glutaraldehyde per ml of PBS, decalcified in 14% EDTA pH 8.0 for 9 days, stained at 30°C in a standard X-gal solution supplemented with 100 mM D-galactose, post-fixed overnight in 10% neutral formalin. Paraffin sections were counterstained with eosin.

#### Smad4

Deparaffinized sections were treated with a MOM kit and then Smad4 mouse monoclonal SC-7966 and DAB reagents which shows Smad4$^{+}$ cells in brown. Sections were counterstained with hematoxylin, which shows all cells in purple.

#### Picrosirius Red

Deparaffinized sections of decalcified bone were stained for 1 hour in 0.1% solution of Sirius Red F3B in saturated picric acid and washed in 0.5% (v/v) glacial acetic acid.

#### Calcein

Intra-peritoneal injections were given 11 and 3 days before euthanasia (15 mg/kg). Non-decalcified bones were embedded in methylmethacrylate.

#### TUNEL

Deparaffinized sections were processed according to manufacturer's directions using *In Situ* Cell Death Detection Kit with Fluorescein (Roche). Sections were mounted with Cytoseal (Thermo Scientific) or Prolong Gold Antifade (Invitrogen). Brightfield and fluorescence microscopy were captured at room temperature with a Nikon Eclipse E600 using a Qimaging ExiBlue camera and Qcapture software; Picrosirius Red with Olympus BX51P polarized light microscope; and whole mounts with a digital camera. Objectives: Nikon 4× /0.13, 10× /0.45 and 40× /0.75.

### High-resolution μCT

Samples from 4-week-old male mice ($n \geq 5$ per genotype), embedded in 2.0% agarose, were scanned post-mortem with a μCT40 (Scanco Medical AG) using 16 μm voxel size, 45 kVp (whole body) or 55 kVp (tibia) of radiation energy, 87 μA (whole body) or 144 μA (tibia) intensity and 300 msecond integration time. For *in vivo* analysis, female mice were anesthetized with isofluorane, and tibiae were scanned using a Viva μCT40 set to 70 kVP and 110 μA. Unless specified otherwise, the first 30 slices below the growth plate were used for trabecular analysis and cortical measurements were assessed using 10 slices at the mathematical midpoint of the tibia.

### Preparation of marrow-free bone tissue and BMSCs

Soft and connective tissue were removed from tibias and femurs of 4-week-old mice and kept in cold PBS during necropsy. A scalpel was used to remove the distal tibia and the proximal femur such that the marrow cavity was exposed. Bones were loaded with cut ends facing down into sterile 0.7 ml microfuge tubes where the bottom of the tube had been pierced with a sterile 18-gauge needle. Bones in 0.7 ml tubes were stacked into sterile 1.5 ml tubes and the multiplex tube assembly was centrifuged at 9000 rpm for 10 seconds at 4°C. Marrow-free bones in 0.7 ml tubes were immediately snap frozen in liquid nitrogen and stored at −80°C. Bone marrow cell pellets in the outer 1.5 ml tubes were used for culture of BMSCs. The marrow pellet was resuspended and incubated for 5 minutes on ice in red blood cell lysis buffer (Roche), washed with ice-cold PBS, resuspended in ascorbic-acid-free α-MEM (Mediatech, Herndon, VA), filtered through a 70 μm cell strainer, and finally resuspended in α-MEM containing 20% fetal calf serum (FCS) and antibiotics. Non-adherent cells were removed by vigorous washing after 3 days of culture.

### Immunoblot and Real-Time quantitative PCR

Frozen, marrow-free bones were pulverized at 2000 rpm for 20 seconds with a Braun Mikrodismembrator, 7 ml shaking flasks and 10 mm chromium steel grinding balls (Sartorius BBI Systems). Shaking flasks and grinding balls were washed in RNase-away soap and were pre-cooled in liquid nitrogen prior to sample processing. For immunoblotting, RIPA buffer (500 µl/bone) was used to collect freshly pulverized bone from shaking flasks. Proteins were separated by SDS-PAGE. Blots represent trends in $n=3$ for $Smad4^{F/F}$, $n=3$ for $Smad4^{+/\Delta}$ and $n=4$ for $Smad4^{\Delta/\Delta}$. For qPCR, Trizol (Invitrogen, 500 µl/bone) was used to collect freshly pulverized bone from shaking flasks. RNA from cultured cells was extracted with RNeasy Plus Kit (Qiagen). Following DNA digestion, RNA was reverse transcribed with oligo dT plus random hexamer primers using EcoDry Premix (Clontech). Data were normalized to *Cyclophilin*, analyzed using the ΔΔCT method and expressed relative to the average of control cells or $Smad4^{F/F}$ samples. $n=7$ for $Smad4^{F/F}$, $n=6$ for $Smad4^{+/\Delta}$ and $n=4$ for $Smad4^{\Delta/\Delta}$. Primers are available upon request.

### Cell culture

Cells were incubated at 37℃ in a humidified atmosphere with 5% $CO_2$ in basic medium [ascorbic-acid-free α-MEM (Invitrogen) plus 10% FBS, 40 mM L-glutamine, 100 U/ml penicillin-G and 100 mg/ml streptomycin], plus osteogenic cocktail (50 µg/ml ascorbic acid, and 10 µM β-glycerophosphate) as indicated. MC3T3 mouse calvaria cells are subclone 4 (ATCC). The adherent fraction of bone marrow cells were seeded at 40,000 cells per well (96-well plate) and cultured for 10–21 days in osteogenic medium ± 200 ng/ml rhBMP2 (Gibco) or 25 ng/ml rmWnt3a (R&D Systems). Primary calvaria were harvested by chopping neonatal calvaria and collecting cells released by 2 hours of incubation in collagenase-A. siRNA (50 nM, Sigma) was transfected with Lipofectamine 2000. MC3T3s were transfected using Lipofectamine 2000 (Invitrogen) for luciferase assays. Transfected cells were treated for 48 hours and analyzed with BrightGlo (Promega). Primary calvaria were seeded to 70% confluence in 96-well dishes, synchronized in cell cycle by overnight deprivation of serum, mitotic cells were labeled for 2 hours with BrdU in serum-free medium ± 200 ng/ml rhBMP2 or 10 ng/ml TGF-β, and quantified with a chemiluminescent cell proliferation ELISA kit (Roche).

To measure apoptosis, primary calvaria were seeded on chamber slides, serum starved overnight ± 200 ng/ml rhBMP2, 25 ng/ml rmWnt3a or 10 ng/ml TGF-β, and stained with *In Situ* Cell Death Detection Kit (Roche) and DAPI. Chromatin immunoprecipitation was carried out on confluent MC3T3s for 72 hours. Extracts were prepared using the SimpleChIP Enzymatic Chromatin IP Kit and magnetic beads (Cell Signaling). EpiTect ChIP qPCR primers targeting the −252 bp region of the murine *Lox* promoter were purchased from Qiagen.

### Statistics

Numerical data are means ± s.e.m. and were compared using the Student's *t*-test for unpaired samples.

## Acknowledgements

Material described here was published in part as a dissertation under United States copyright #TX6-736-939. We thank Dr Dave Beebe for *Smad4* mice, Dr Vicki Rosen (Harvard University) for support during preparation of this manuscript, Drs Deborah Novack and Audrey MacAlinden (Washington University) for comments and critiques, and Sung Yeop Joeng for assistance with osteocyte density. R. Civitelli is a shareholder of Eli-Lilly, Merck and Amgen, and received grant support from Amgen and Pfizer.

## Author contributions

This work was conceived, designed and interpreted by V.S.S., G.M. and R.C. Work was performed in entirety at Washington University School of Medicine in St Louis by V.S.S., N.Z., L.H., J.N., G.M. and R.C.

## Funding

This work was supported by the National Institutes of Health [grant numbers R01-AR056678 and R01-AR055913 to R.C., F31-AR056586 to V.S.S.]; the Research Center for Auditory and Vestibular Studies [grant number P30-DC004665]; the Washington University Center for Musculoskeletal Biology and Medicine [grant number P30-AR057235]; and the Barnes-Jewish Hospital Foundation (to R.C.). Deposited in PMC for release after 12 months.

Supplementary material available online at
http://jcs.biologists.org/lookup/suppl/doi:10.1242/jcs.131953/-/DC1

## References

**Bain, G., Müller, T., Wang, X. and Papkoff, J.** (2003). Activated β-catenin induces osteoblast differentiation of C3H10T1/2 cells and participates in BMP2 mediated signal transduction. *Biochem. Biophys. Res. Commun.* **301**, 84-91.

**Bandyopadhyay, A., Tsuji, K., Cox, K., Harfe, B. D., Rosen, V. and Tabin, C. J.** (2006). Genetic analysis of the roles of BMP2, BMP4, and BMP7 in limb patterning and skeletogenesis. *PLoS Genet.* **2**, e216.

**Batlle, E., Henderson, J. T., Beghtel, H., van den Born, M. M., Sancho, E., Huls, G., Meeldijk, J., Robertson, J., van de Wetering, M., Pawson, T. et al.** (2002). β-catenin and TCF mediate cell positioning in the intestinal epithelium by controlling the expression of EphB/ephrinB. *Cell* **111**, 251-263.

**Beighton, P., De Paepe, A., Steinmann, B., Tsipouras, P., Wenstrup, R. J.; Ehlers-Danlos National Foundation (USA) and Ehlers-Danlos Support Group (UK)** (1998). Ehlers-Danlos syndromes: revised nosology, Villefranche, 1997. *Am. J. Med. Genet.* **77**, 31-37.

**Boyden, L. M., Mao, J., Belsky, J., Mitzner, L., Farhi, A., Mitnick, M. A., Wu, D., Insogna, K. and Lifton, R. P.** (2002). High bone density due to a mutation in LDL-receptor-related protein 5. *N. Engl. J. Med.* **346**, 1513-1521.

**Chen, Y., Whetstone, H. C., Youn, A., Nadesan, P., Chow, E. C., Lin, A. C. and Alman, B. A.** (2007). β-catenin signaling pathway is crucial for bone morphogenetic protein 2 to induce new bone formation. *J. Biol. Chem.* **282**, 526-533.

**Cong, F., Schweizer, L., Chamorro, M. and Varmus, H.** (2003). Requirement for a nuclear function of beta-catenin in Wnt signaling. *Mol. Cell. Biol.* **23**, 8462-8470.

**Davey, R. A., Clarke, M. V., Sastra, S., Skinner, J. P., Chiang, C., Anderson, P. H. and Zajac, J. D.** (2012). Decreased body weight in young Osterix-Cre transgenic mice results in delayed cortical bone expansion and accrual. *Transgenic Res.* **21**, 885-893.

**Day, T. F., Guo, X., Garrett-Beal, L. and Yang, Y.** (2005). Wnt/β-catenin signaling in mesenchymal progenitors controls osteoblast and chondrocyte differentiation during vertebrate skeletogenesis. *Dev. Cell* **8**, 739-750.

**Dayan, D., Hiss, Y., Hirshberg, A., Bubis, J. J. and Wolman, M.** (1989). Are the polarization colors of picrosirius red-stained collagen determined only by the diameter of the fibers? *Histochemistry* **93**, 27-29.

**Di Benedetto, A., Watkins, M., Grimston, S., Salazar, V., Donsante, C., Mbalaviele, G., Radice, G. L. and Civitelli, R.** (2010). N-cadherin and cadherin 11 modulate postnatal bone growth and osteoblast differentiation by distinct mechanisms. *J. Cell Sci.* **123**, 2640-2648.

**Diarra, D., Stolina, M., Polzer, K., Zwerina, J., Ominsky, M. S., Dwyer, D., Korb, A., Smolen, J., Hoffmann, M., Scheinecker, C. et al.** (2007). Dickkopf-1 is a master regulator of joint remodeling. *Nat. Med.* **13**, 156-163.

**Ducy, P. and Karsenty, G.** (1995). Two distinct osteoblast-specific cis-acting elements control expression of a mouse osteocalcin gene. *Mol. Cell. Biol.* **15**, 1858-1869.

**Forlino, A., Cabral, W. A., Barnes, A. M. and Marini, J. C.** (2011). New perspectives on osteogenesis imperfecta. *Nat. Rev. Endocrinol.* **7**, 540-557.

**Glass, D. A., 2nd, Bialek, P., Ahn, J. D., Starbuck, M., Patel, M. S., Clevers, H., Taketo, M. M., Long, F., McMahon, A. P., Lang, R. A. et al.** (2005). Canonical Wnt signaling in differentiated osteoblasts controls osteoclast differentiation. *Dev. Cell* **8**, 751-764.

**Gong, Y., Vikkula, M., Boon, L., Liu, J., Beighton, P., Ramesar, R., Peltonen, L., Somer, H., Hirose, T., Dallapiccola, B. et al.** (1996). Osteoporosis-pseudoglioma syndrome, a disorder affecting skeletal strength and vision, is assigned to chromosome region 11q12-13. *Am. J. Hum. Genet.* **59**, 146-151.

**Gong, Y., Slee, R. B., Fukai, N., Rawadi, G., Roman-Roman, S., Reginato, A. M., Wang, H., Cundy, T., Glorieux, F. H., Lev, D. et al.; Osteoporosis-Pseudoglioma Syndrome Collaborative Group** (2001). LDL receptor-related protein 5 (LRP5) affects bone accrual and eye development. *Cell* **107**, 513-523.

**Greenblatt, M. B., Shim, J. H., Zou, W., Sitara, D., Schweitzer, M., Hu, D., Lotinun, S., Sano, Y., Baron, R., Park, J. M. et al.** (2010). The p38 MAPK pathway is essential for skeletogenesis and bone homeostasis in mice. *J. Clin. Invest.* **120**, 2457-2473.

**Hill, T. P., Später, D., Taketo, M. M., Birchmeier, W. and Hartmann, C.** (2005). Canonical Wnt/β-catenin signaling prevents osteoblasts from differentiating into chondrocytes. *Dev. Cell* **8**, 727-738.

**Hu, H., Hilton, M. J., Tu, X., Yu, K., Ornitz, D. M. and Long, F.** (2005). Sequential roles of Hedgehog and Wnt signaling in osteoblast development. *Development* **132**, 49-60.

**Hunter, I., McGregor, D. and Robins, S. P.** (2001). Caspase-dependent cleavage of cadherins and catenins during osteoblast apoptosis. *J. Bone Miner. Res.* **16**, 466-477.

**Kamiya, N., Ye, L., Kobayashi, T., Lucas, D. J., Mochida, Y., Yamauchi, M., Kronenberg, H. M., Feng, J. Q. and Mishina, Y.** (2008a). Disruption of BMP signaling in osteoblasts through type IA receptor (BMPRIA) increases bone mass. *J. Bone Miner. Res.* **23**, 2007-2017.

**Kamiya, N., Ye, L., Kobayashi, T., Mochida, Y., Yamauchi, M., Kronenberg, H. M., Feng, J. Q. and Mishina, Y.** (2008b). BMP signaling negatively regulates bone mass through sclerostin by inhibiting the canonical Wnt pathway. *Development* **135**, 3801-3811.

**Kang, Q., Sun, M. H., Cheng, H., Peng, Y., Montag, A. G., Deyrup, A. T., Jiang, W., Luu, H. H., Luo, J., Szatkowski, J. P. et al.** (2004). Characterization of the distinct orthotopic bone-forming activity of 14 BMPs using recombinant adenovirus-mediated gene delivery. *Gene Ther.* **11**, 1312-1320.

**Little, R. D., Carulli, J. P., Del Mastro, R. G., Dupuis, J., Osborne, M., Folz, C., Manning, S. P., Swain, P. M., Zhao, S. C., Eustace, B. et al.** (2002). A mutation in

the LDL receptor-related protein 5 gene results in the autosomal dominant high-bone-mass trait. *Am. J. Hum. Genet.* **70**, 11-19.

**Maes, C., Kobayashi, T., Selig, M. K., Torrekens, S., Roth, S. I., Mackem, S., Carmeliet, G. and Kronenberg, H. M.** (2010). Osteoblast precursors, but not mature osteoblasts, move into developing and fractured bones along with invading blood vessels. *Dev. Cell* **19**, 329-344.

**Mishina, Y., Starbuck, M. W., Gentile, M. A., Fukuda, T., Kasparcova, V., Seedor, J. G., Hanks, M. C., Amling, M., Pinero, G. J., Harada, S. et al.** (2004). Bone morphogenetic protein type IA receptor signaling regulates postnatal osteoblast function and bone remodeling. *J. Biol. Chem.* **279**, 27560-27566.

**Mundlos, S., Otto, F., Mundlos, C., Mulliken, J. B., Aylsworth, A. S., Albright, S., Lindhout, D., Cole, W. G., Henn, W., Knoll, J. H. et al.** (1997). Mutations involving the transcription factor CBFA1 cause cleidocranial dysplasia. (see comments). *Cell* **89**, 773-779.

**Nishioka, T., Eustace, A. and West, C.** (2012). Lysyl oxidase: from basic science to future cancer treatment. *Cell Struct. Funct.* **37**, 75-80.

**Nusse, R.** (2005). Wnt signaling in disease and in development. *Cell Res.* **15**, 28-32.

**Otto, F., Thornell, A. P., Crompton, T., Denzel, A., Gilmour, K. C., Rosewell, I. R., Stamp, G. W., Beddington, R. S., Mundlos, S., Olsen, B. R. et al.** (1997). Cbfa1, a candidate gene for cleidocranial dysplasia syndrome, is essential for osteoblast differentiation and bone development. (see comments). *Cell* **89**, 765-771.

**Pischon, N., Mäki, J. M., Weisshaupt, P., Heng, N., Palamakumbura, A. H., N'Guessan, P., Ding, A., Radlanski, R., Renz, H., Bronckers, T. A. et al.** (2009). Lysyl oxidase (lox) gene deficiency affects osteoblastic phenotype. *Calcif. Tissue Int.* **85**, 119-126.

**Rawadi, G., Vayssière, B., Dunn, F., Baron, R. and Roman-Roman, S.** (2003). BMP-2 controls alkaline phosphatase expression and osteoblast mineralization by a Wnt autocrine loop. *J. Bone Miner. Res.* **18**, 1842-1853.

**Retting, K. N., Song, B., Yoon, B. S. and Lyons, K. M.** (2009). BMP canonical Smad signaling through Smad1 and Smad5 is required for endochondral bone formation. *Development* **136**, 1093-1104.

**Rodda, S. J. and McMahon, A. P.** (2006). Distinct roles for Hedgehog and canonical Wnt signaling in specification, differentiation and maintenance of osteoblast progenitors. *Development* **133**, 3231-3244.

**Ross, S. E., Hemati, N., Longo, K. A., Bennett, C. N., Lucas, P. C., Erickson, R. L. and MacDougald, O. A.** (2000). Inhibition of adipogenesis by Wnt signaling. *Science* **289**, 950-953.

**Salazar, V. S., Mbalaviele, G. and Civitelli, R.** (2008). The pro-osteogenic action of β-catenin requires interaction with BMP signaling, but not Tcf/Lef transcriptional activity. *J. Cell. Biochem.* **104**, 942-952.

**Salo, A. M., Cox, H., Farndon, P., Moss, C., Grindulis, H., Risteli, M., Robins, S. P. and Myllylä, R.** (2008). A connective tissue disorder caused by mutations of the lysyl hydroxylase 3 gene. *Am. J. Hum. Genet.* **83**, 495-503.

**Soriano, P.** (1999). Generalized lacZ expression with the ROSA26 Cre reporter strain. *Nat. Genet.* **21**, 70-71.

**Tan, X., Weng, T., Zhang, J., Wang, J., Li, W., Wan, H., Lan, Y., Cheng, X., Hou, N., Liu, H. et al.** (2007). Smad4 is required for maintaining normal murine postnatal bone homeostasis. *J. Cell Sci.* **120**, 2162-2170.

**Tetsu, O. and McCormick, F.** (1999). β-catenin regulates expression of cyclin D1 in colon carcinoma cells. *Nature* **398**, 422-426.

**Trackman, P. C.** (2005). Diverse biological functions of extracellular collagen processing enzymes. *J. Cell. Biochem.* **96**, 927-937.

**Winkler, D. G., Sutherland, M. S., Ojala, E., Turcott, E., Geoghegan, J. C., Shpektor, D., Skonier, J. E., Yu, C. and Latham, J. A.** (2005). Sclerostin inhibition of Wnt-3a-induced C3H10T1/2 cell differentiation is indirect and mediated by bone morphogenetic proteins. *J. Biol. Chem.* **280**, 2498-2502.

**Wozney, J. M., Rosen, V., Celeste, A. J., Mitsock, L. M., Whitters, M. J., Kriz, R. W., Hewick, R. M. and Wang, E. A.** (1988). Novel regulators of bone formation: molecular clones and activities. *Science* **242**, 1528-1534.

**Zhang, J., Tan, X., Li, W., Wang, Y., Wang, J., Cheng, X. and Yang, X.** (2005). Smad4 is required for the normal organization of the cartilage growth plate. *Dev. Biol.* **284**, 311-322.